T2SL production and development at IRnova – from MWIR to VLWIR detection

L. Höglund, R. Marcks von Würtemberg, C. Asplund, H. Kataria, A. Gamfeldt, E. Costard

IRnova AB, Isafjordsgatan 22 C5, SE-16440 Kista, Sweden

ABSTRACT

Development towards higher operating temperature, smaller pitch and larger format arrays is ongoing for midwave (MW) InAs/GaSb superlattice detectors at IRnova. One part of this effort entails improvement in the MW detector design, which has resulted in increased quantum efficiency to 55-60 % in the entire 3-5 µm wavelength region, with dark current levels lower than 3×10^{-6} A/cm^2 at 120 K. Furthermore, MW-MW dual band detectors have been realized by using pixel filters fabricated on top of regular MW FPAs. The pixel filters were designed to transmit infrared radiation in the 3.5 µm - 4.1 µm wavelength region and to completely block light shorter than 3.5 µm. By comparing the signals of filtered and unfiltered pixels, excellent contrast between the two bands were obtained. Long wave infrared detectors have also been realized with cut-off wavelength at 12.2 µm and dark current levels following the Rule07 trendline from 80 K to 160 K, with only two times higher dark current than Rule07 at 80 K.

Keywords: heterostructure, infrared, detector, superlattice, InAs/GaSb

1. INTRODUCTION

InAs/InGaSb Type-II superlattices (T2SLs) have proven to be excellent material for high end infrared (IR) detectors, with good manufacturability and exceptional long term stability [1,2]. Both mid wave infrared (MWIR, 3-5 µm) and long-wave infrared (LWIR, 8-12 µm) detectors based on T2SLs are mature enough to be manufactured by several companies [3]. Strong reduction of the generation-recombination (G-R) dark current has been demonstrated, which results in improved detector performance [4,5,6,7,8,9]. One of the main reasons for the rapid improvement in detector performance is the novel barrier designs that utilize wide bandgap barriers to block the flow of majority carriers while allowing unimpeded transport of the minority carriers [10,11,12].

In this paper, results from our enhanced MW detector design are presented with quantum efficiency (QE) values > 55% in the entire 3-5 µm region and dark current density < 3×10^{-6} A/cm^2 at 120K. Furthermore, we present results from a MW/MW dual color focal plane array (FPA), which was designed to enhance the sensitivity to volatile organic compound (VOC) gases. A broadband MWIR superlattice FPA was used and a pixel filter with transmission in the 3.5-4.1 µm wavelength band was fabricated on top of the thinned down array in a checker board pattern. As a result, radiation from the VOC gas band was absorbed by the unfiltered pixels only, while the filtered pixels were used as reference pixels. By combining the information from the filtered and unfiltered pixels the gas contrast was greatly enhanced. For LWIR detectors with cut-off wavelength at 12.2 µm, dark current values only 2 times higher than Rule07 have been observed at 80K.

2. EXPERIMENTAL DETAILS

2.1 Material

Three structures with different cut-off wavelengths are presented in this paper, two MWIR structures: Structure A with 5.1 µm cut-off wavelength and structure B, with 5.5 µm cut-off wavelength (at 80 K) and one LWIR structure (12.2 µm cut-off wavelength at 80 K). The MWIR structures (schematically illustrated in Figure 1) are slightly modified and improved versions of the epitaxial design reported in [13], that has been described in full detail in [14]. A similar design as shown in Figure 1 was used for the LWIR detectors, but with the InAs, GaSb and AlSb layer thicknesses of the SLs slightly modified to change the bandgaps to the desired wavelength regions.

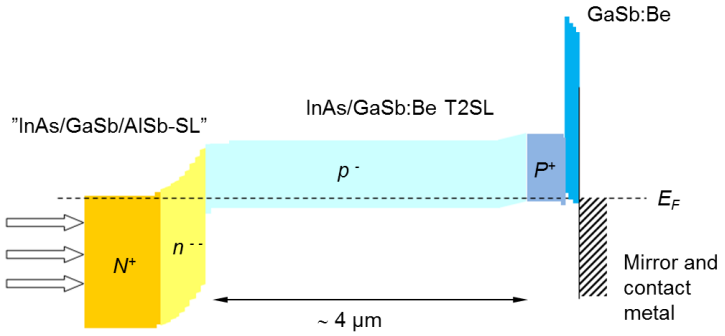

Figure 1. Double heterostructure (DH) detector design used in IRnova's detectors

2.2 Fabrication

LWIR and MWIR single pixel devices and MWIR FPAs were fabricated using standard III/V processing techniques. Stepper lithography was used to define the pixels. Pixels were formed by a combination of dry and wet etching [15] and passivated using a dielectric passivation [16]. Mirror, contact metal and indium bumps were evaporated onto the pixels before dicing. The arrays were then hybridized to read out integrated circuits (ROICs), underfill was deposited and finally the GaSb substrate was fully removed. For the dual color FPA, a pixel filter was deposited and patterned in a checker board pattern, leaving the pixel filter on every second pixel.

3. RESULTS

3.1 Dual color detectors based on 320 × 256 MWIR FPAs with fabricated pixel filters

The FPAs used for dual color detection were based on a MWIR T2SL optimized for VOC detection at 3.3 µm. Photodiodes based on this material show good performance, both in terms of quantum efficiency (QE**)** and dark current**.** The QE in the gas band (3-3.5 µm) was ~40-50% at 3.3 µm, without AR-coating (Figure 2a). The detectors are backside illuminated, with a highly reflective top contact, so they benefit from a double pass of the incident IR radiation. A temperature dependence of the QE is observed, which is attributed to a limited diffusion length in the devices [1,17]. In section 3.2, detector results from an enhanced design (Structure B) are presented in which the diffusion length has been extended to further enhance the QE. The dark current density at -0.05 V operating bias is $\leq 1 \times 10^{-6}$ A/cm^2 for all temperatures ≤ 120 K (Figure 2b), which allows for high temperature operation.

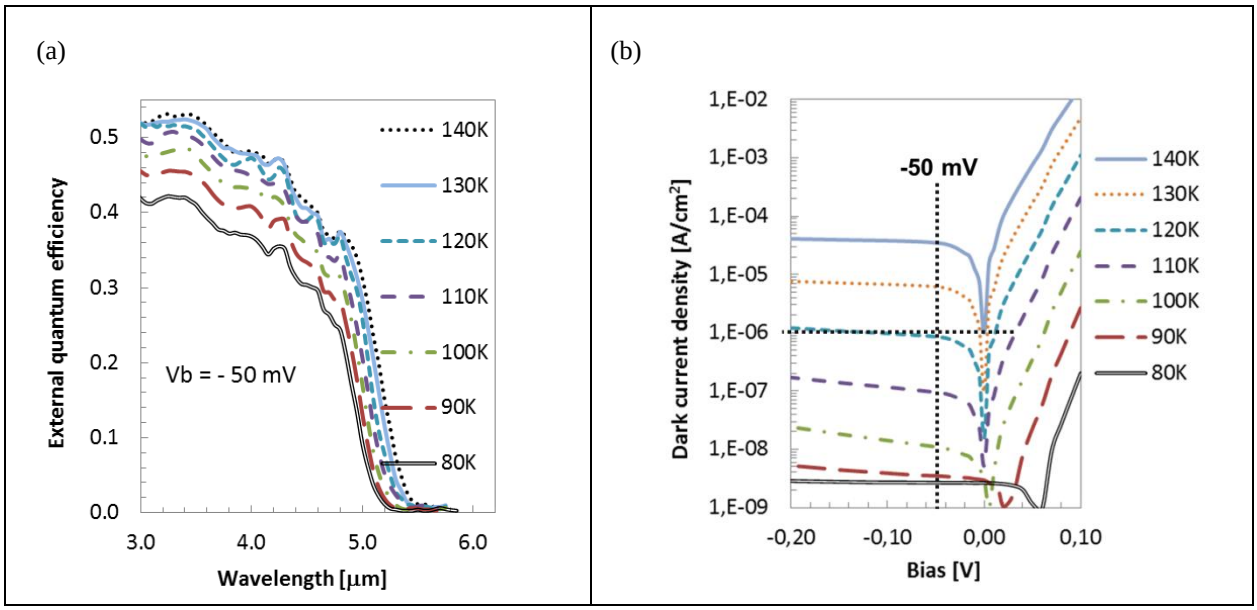

Figure 2. (a) Detector quantum efficiency at an applied bias of -50 mV and (b) dark current density in the temperature range T = 80 – 140 K

For the dual color FPAs, filters were deposited on fabricated MWIR FPAs as well as on plain reference wafers. The reference wafers were used to deduce the transmission of the filter. In these measurements, full blocking of the gas band and high transmission in the reference band were observed (Figure 3). Good agreement was also obtained between the measured and calculated transmission spectra.

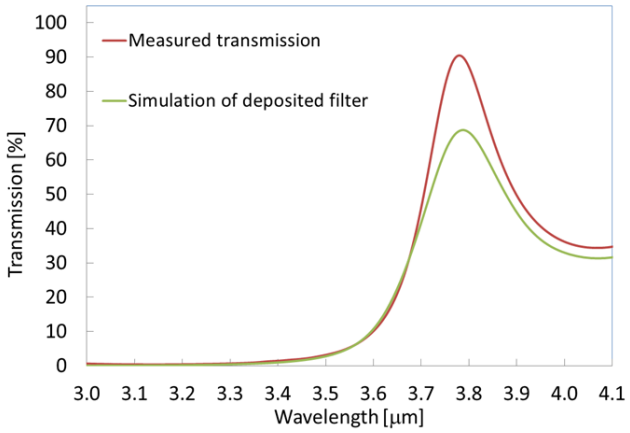

Figure 3. Measured transmission spectra of the pixel filter deposited on the array compared to the fitted calculation.

The pixel filter deposited on the arrays was patterned and etched in a checker board pattern (Figure 4a). To demonstrate the ability to distinguish gases with this FPA, an image was taken using a basic lens setup looking at a nozzle of a gas bottle (see Figure 4b). Standard gain and offset corrections were performed when no gas was present. Consequently, when looking at a uniform target with no absorbing gas present, all pixels in the array are expected to have the same signal level. The bottle containing pure butane gas was opened very slightly to give a small flow of gas out of the nozzle. In this image, the expected checkerboard pattern appears in the gas cloud exiting the nozzle, differentiating it from the background where no gas was present. No bad pixel replacement was implemented which is why some black and white pixels are still present in the image.

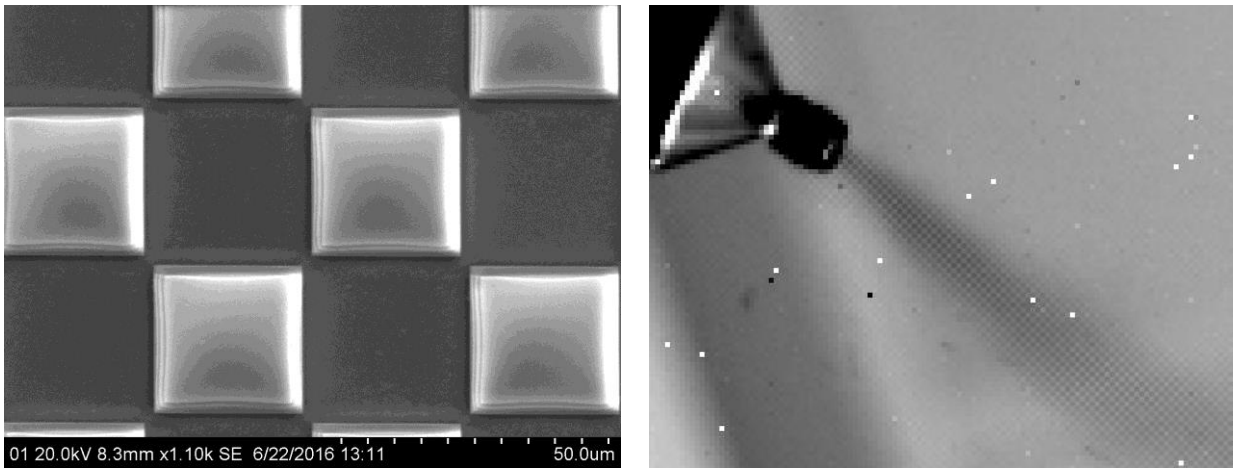

Figure 4. (a) SEM image showing the checker board patterned pixel filters (b) Image of butane gas flowing from a bottle, showing the checkered pattern in the image were the gas affects the signal of the filtered and unfiltered pixels differently.

In a second test, images were collected from the arrays facing different extended black body targets. Also available in this setup was a gas cell, enabling the controlled introduction of gas in the path between the temperature controlled black body background and the detector. The distributions of pixel signals with and without butane gas present were compared (Figure 5). When the gas cell is filled with butane gas (at room temperature), two different distributions were seen, representing the filtered and non-filtered sets of pixels (Figure 5a). In contrast, when the gas cell is filled with N_2 (a gas with no absorption in the spectral range of the detector), all pixels were distributed around a single value **(**Figure 5b**).** These results demonstrate that the pixel filters worked as designed. A more detailed description of this dual color camera has been given in one of our previous publications [18].

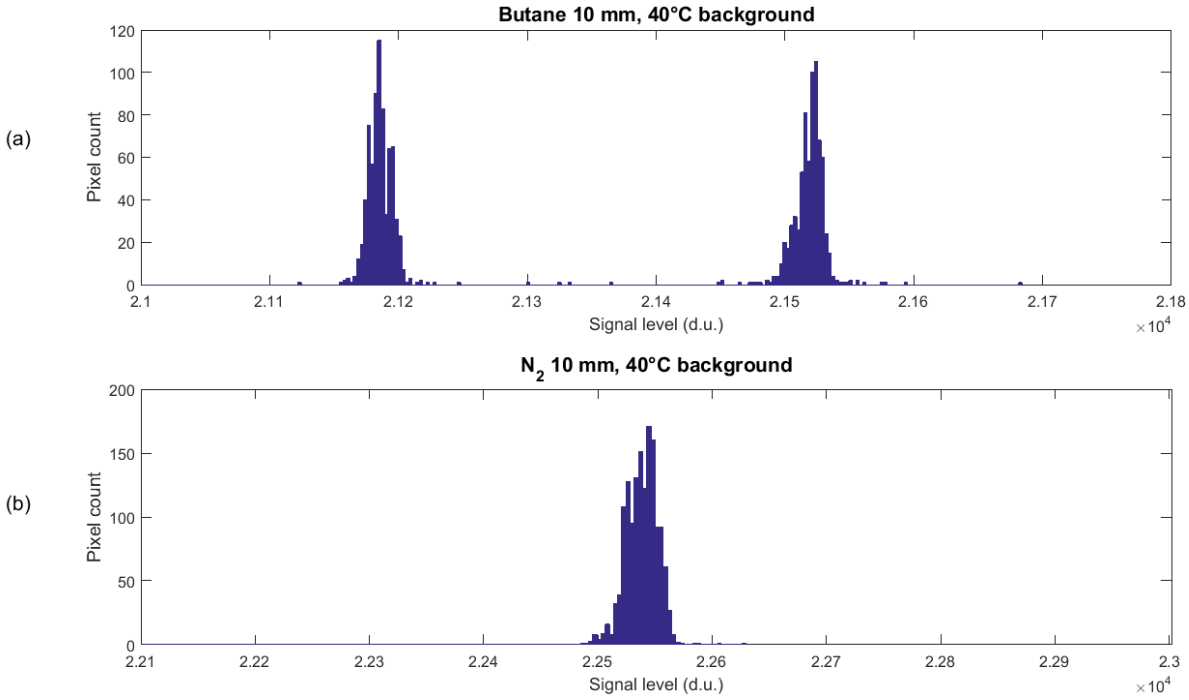

Figure 5. (a) Distribution of pixel values with butane gas present (b) Distribution of pixel values with N_2 gas present. In both cases a 40°C black body source was imaged.

3.2 Development of 640 × 512 MWIR detectors

Work is in progress to launch a second generation of 640 × 512 MWIR FPAs with 15 µm pitch. In order to keep a high photocurrent even at a smaller pitch, the detector design (Structure B) has been modified to cover the full MWIR spectrum and to further improve the QE. With the design changes performed in structure B, the cutoff wavelength is increased to 5.5 µm and QE values > 55% are observed in the entire 3-5 µm range (Figure 6a). (a). Very little temperature dependence of the quantum efficiency is observed for Structure B, indicating that the diffusion length is no longer a limiting factor for the QE in the new design. In addition, the detector is fully turned on at 0 V bias, resulting in a spectral QE that is independent of applied bias (Figure 6c). A minor increase of the dark current is observed with the new design (structure B), but the levels are still low, on the order of 3×10^{-6} at 120K (Figure 6b).

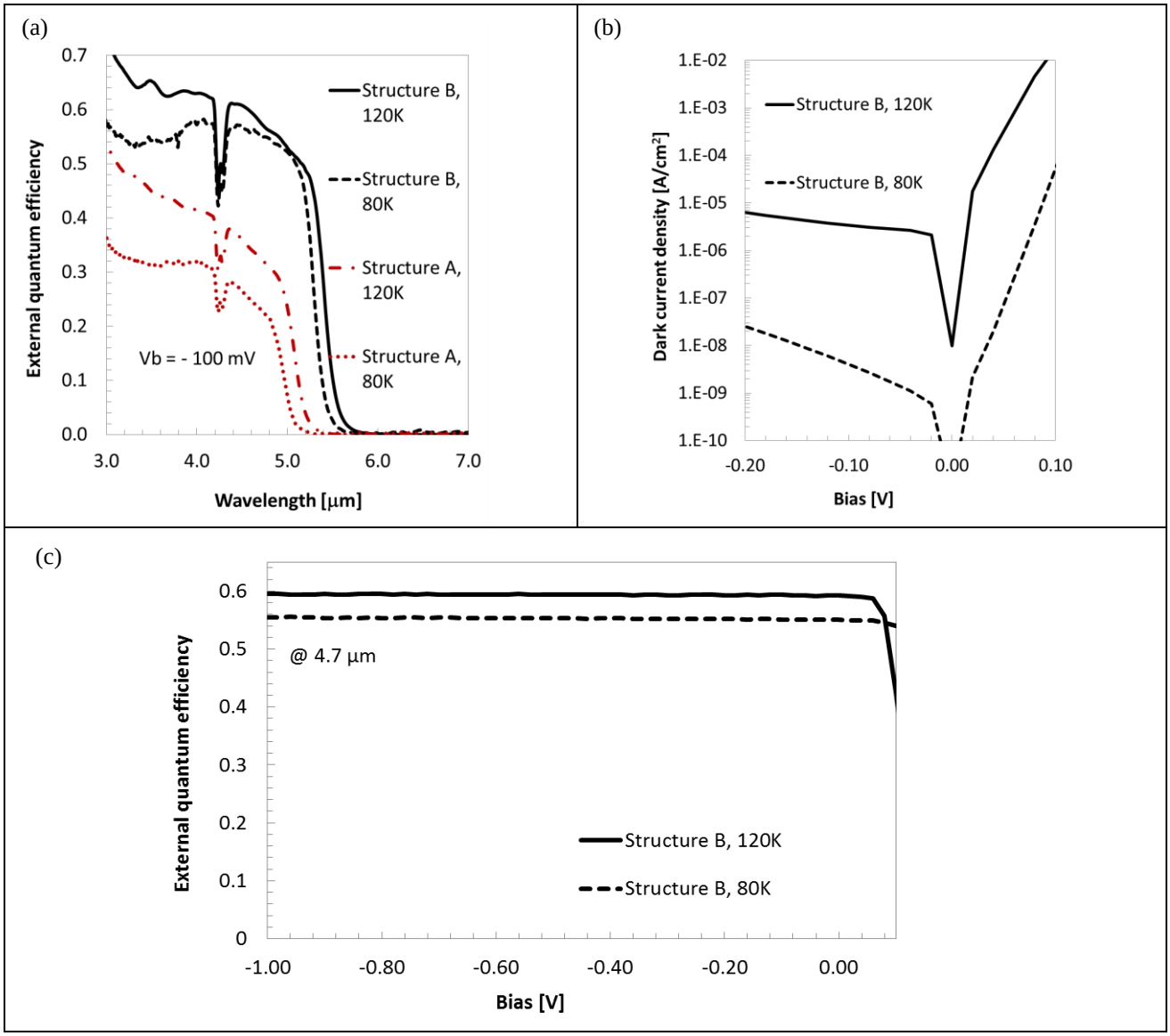

Figure 6. (a) Comparison of the detector quantum efficiencies for Structure A and Structure B at an applied bias of -100 mV and (b) Dark current densities for the Structure B at T = 80 K and 120 K (c) Bias dependence of the detector quantum efficiency of structure B (at 4.7 µm).

3.3 LWIR and VLWIR detectors

Large size 2D arrays for detection up to about 16 µm are mandatory for future space applications, particularly for weather forecast and atmospheric sounding missions. For these missions both high QE and low dark current are required. Mercury-Cadmium-Telluride (MCT) is currently the detector of choice for these applications, however the operability of MCT arrays in this wavelength region is low and the performance of operable pixels degrade with time. T2SL is recognized as the most promising alternative to MCT for 2D LWIR and very long wave infrared (VLWIR, ~12 - 30 µm) array production, and would presumably give better uniformity and operability. IRnova is currently developing detectors for these applications, starting with LWIR detectors with 12 µm cut-off wavelength. Results from single pixel detectors are very promising with dark current values only 2-3 times higher than Rule07 for temperatures > 80 K (Figure 7). For temperatures < 80 K, the dark current is still decreasing, showing that the dark current is not dominated by surface leakage current. Furthermore, the turn on bias of the detector response is very low < 25 mV (Figure 8). The next step is to adapt the FPA processing to these cut-off wavelengths and then to extend the cut-off wavelengths to 14.5 µm and 16.5 µm.

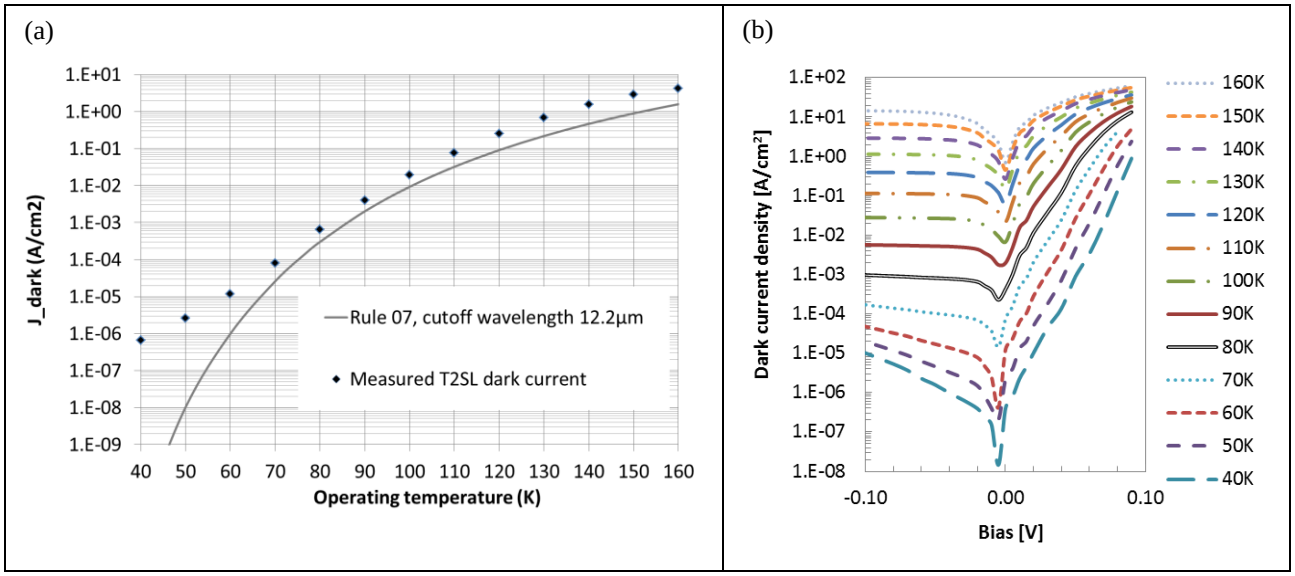

Figure 7. Dark current of a 12.2 µm T2SL LWIR detector (a) Comparison of dark current density at -0.05 V with Rule07 shows that the dark current density is only 2-3 times higher than Rule07 at temperatures ≥ 80 K (b) Dark current density vs applied bias in the temperature range 40 K – 160 K for a 90 µm × 90 µm single pixel device.

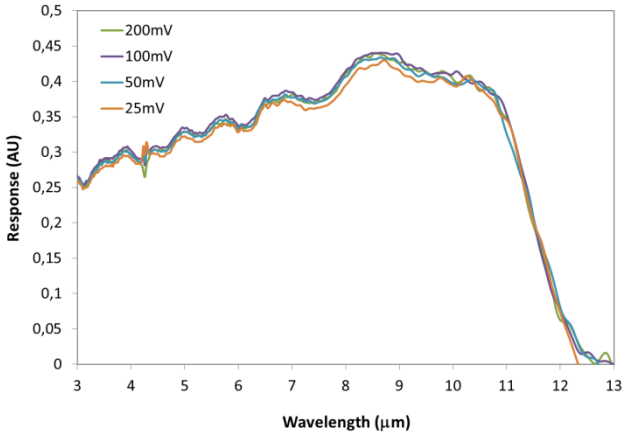

Figure 8. Response of the 12.2 µm T2SL LWIR detector operated at 77K.

3.4 Integrated dewar cooler assembly

The majority of the T2SL and QWIP detectors manufactured at IRnova now utilize the same kind of integrated dewar cooler assembly (IDCA), with the same external mechanical and electrical interface independent of the FPA format (Figure 9). This enables drop-in replacement between IDCAs based on either 320 × 256 FPAs, 640 × 512 FPAs or dual-color FPAs. The IDCA can also be customized with cold filters optimized for optical gas imaging (e.g. for VOC gases like methane and butane in MWIR and for SF6 and Ammonia in LWIR + many others). A summary of the power consumption, NETD, frame rates and f-numbers for different formats are summarized in table 1.

.

Figure 9. Integrated dewar cooler assembly.

Table 1. Summary of the performance of different IDCAs manufactured at IRnova.

IDCA PARAMETERS				
IDCA Type	**IRnova 640-LW**	**IRnova 320ER-LW**	**IRnova 640-MW**	**IRnova 320ER-MW**
Detector Type	QWIP	QWIP	T2SL	T2SL
Resolution	640 x 512	320 x 256	640 x 512	320 x 256
Pixel Pitch	15 µm	30 µm	15 µm	30 µm
Spectral Range	~ 7.5 – 9.0 µm	~ 7.5 – 9.0 µm	~ 3.5 – 5.0 µm	~ 3.5 – 5.0 µm
F-number	F# 2 (F# 4 option available in MWIR)			
Temporal NETD	~ 25 mK	~ 25 mK	~ 20 mK	~ 12 mK
Spatial NETD	~ 10 mK	~ 10 mK	~ 10 mK	~ 4 mK
Operability	~ 99.9%	~ 99.9%	~ 99.9 %	~ 99.9 %
Frame rate	Max. 60 Hz (selectable framerate supported)			
Input power	~ 7 W			
Cool Down Time	~ 6 min			
Supply Voltage	12 V			
Elec. Interfaces	LVDS and I^2C			
Weight	~ 550 g			

4. SUMMARY

In this article, results from InAs/GaSb superlattice detectors for midwave, longwave and midwave-midwave dual color detection have been presented. A new detector design have been implemented for midwave detectors, resulting in quantum efficiency values of 55 - 60 % in the entire 3-5 µm wavelength region and dark current values < 3×10^{-6} A/cm^2 for temperatures < 120 K. FPA results from a dual color detectors with pixel filters on every second pixel have been demonstrated with excellent contrast between filtered and unfiltered pixels. Low dark current and low turn-on bias have been observed for LWIR detectors with cut-off wavelength at 12.2 µm.

5. ACKNOWLEDGEMENTS

We would like to thank ESA for sponsoring work on VLWIR superlattice detectors in the project Low Dark current VLWIR T2SL infrared detectors.

REFERENCES

[1] Höglund, L., Asplund, C., Marcks von Würtemberg, R., Kataria, H., Gamfeldt, A., Smuk, S., Costard, E., "Manufacturability of type-II InAs/GaSb superlattice detectors for infrared imaging", Infrared Physics & Technology, Available online 6 March 2017, http://dx.doi.org/10.1016/j.infrared.2017.03.002

[2] Nghiem, J, Jaeck, J., Giard, E., Caes, M., Rodriguez, J. B., Christol, P., Haidar, R., Costard, E., Ribet-Mohamed, I., "MTF and FPN measurements to evaluate midwave infrared T2SL focal plane arrays**"**
Proc. SPIE. 10111, Quantum Sensing and Nano Electronics and Photonics XIV, 101111D. (January 27, 2017)

[3] AIM (www.aim-ir.com), IRnova (www.ir-nova.se), SCD (www.scd.co.il), Qmagic (www.qmagic.com)

[4] Vurgaftman, I., Aifer, E., Canedy, C., Tischler, J., Meyer, J., Warner, J., Jackson, E., Hildebrandt, G., Sullivan, G., "Graded bandgap for dark current suppression in long-wave infrared W-structured type-II Superlattice photodiodes", Appl. Phys. Lett. 89 (12) 121114 (2006)

[5] Soibel, A., Rafol, S. B., Khoshakhlagh, A., Nguyen, J., Hoeglund, L., Keo, S. A., Mumolo, J. M., Liu, J., Liao, A., Ting, D. Z. Y., Gunapala, S. D., "Long wavelength infrared Superlattice detectors and FPAs based on CBIRD design", IEEE Photonics Technol. Lett. 25 (9) 875-878 (2013).

[6] Fuchs, F., Weimer, U., Pletschen, W., Schmitz, J., Ahlswere, E., Walter, M., Wagner, J., and Koidl, P., "High performance Superlattice infrared photodiodes", Appl. Phys. Lett. **71**(22), 3251-3253 (1997)

[7] Aifer, E. H., Tischler, J. G., Warner, J. H., Vurgaftman, I., Bewley, W. W., Meyer, J. R., Kim, J. C., Whitman, L. J., Canedy, C. L., and Jackson, E. M., "W-structured type-II long-wave infrared photodiodes with high quantum efficiency"Appl. Phys. Lett. **89**, 053519 (2006)

[8] Nguyen, B. –M., Hoffman, D., Delaunay, P. –Y. and Razeghi, M., "nBn detector, an infrared photodetector with reduced dark current and higher operating temperature",Appl. Phys. Lett. **91**(16) 163511 (2007)

[9] Ting, D. Z. –Y., Hill, C. J., Soibel, A., Keo, S., Mumolo, J.M., Nguyen, J., and Gunapala, S. D., "A high-performance long wavelength superlattice complementary barrier infrared photodetector "Appl. Phys. Lett. **95**(2), 023508 (2009)

[10] White, A. M., "Infrared detectors", USA Patent 4,679,063 (1987)

[11] Maimon, S. and Wicks, G. W., " detector, an infrared detector with reduced dark current and higher operating temperature", Appl. Phys. Lett. 89, 151109 (2006)

[12] Klipstein, P., ""XBn " barrier photodetectors for high sensitivity and high operating temperature infrared sensors", Proc. of SPIE, 6940, 151109 (2009)

[13] Asplund, C., Marcks von Würtemberg, R., Lantz, D., Malm, H., Martijn, H., Plis, E., Gautam, N. and Krishna, S., "Performance of mid-wave T2SL detectors with heterojunction barriers", Infrared Physics & Technology 59 (2013) 22–27.

[14] Malm, H., Gamfeldt, A., Marcks von Würtemberg, R., Lantz, D., Asplund, C., Martijn, H., "High image quality type-II Superlattice detector for 3.3 µm detection of volatile organic compounds", Infrared Physics & Technology 70, 34–39 (2015)

[15] Chaghi, R., Cervera, C., Aït-Kaci, H., Grech, P., Rodriguez, J. B. and Christol, P., "Wet etching and chemical polishing of InAs / GaSb superlattice photodiodes", Semicond. Sci. Technol. 24, 065010 (2009).

[16] Martijn, H., Asplund, C., Marcks von Würtemberg, R. and Malm, H.,"High performance MWIR type-II superlattice detectors", Infrared Technology and Applications XXXIX, Proc. of SPIE Vol. 8704, 87040Z (2013).

[17] Asplund, C., Marcks von Würtemberg, R., Höglund, L., "Modeling Tools For Design Of Type-II Superlattice Photodetectors", Infrared Physics & Technology, Available online 9 March 2017, http://dx.doi.org/10.1016/j.infrared.2017.03.006

[18] Höglund, L., Marcks von Würtemberg, R, Gatty, H., Gamfeldt, A., Asplund, C., Costard, E. "Type-II InAs/GaSb superlattices for dual color infrared detection**"**, Proc. SPIE 10111, Quantum Sensing and Nano Electronics and Photonics XIV, 1011116 (27 January 2017)